Optical and thermal properties of Sb/Bi-modified mixed Ge-Ga-Se-Te glasses

R. Golovchak, A. Kozdras, T. Hodge, J. Szlęzak, Catherine Boussard-Plédel,
Y. Shpotyuk, B. Bureau

Optical and thermal properties of Sb/Bi-modified mixed Ge-Ga-Se-Te glasses

R. Golovchak[1], A. Kozdras[2], T. Hodge[1], J. Szlęzak[3,4], C. Boussard-Pledel[4],

Ya. Shpotyuk[3,5,*], B. Bureau[4]

[1] *Department of Physics and Astronomy, Austin Peay State University, Clarksville, TN 37044, USA*

[2] *Faculty of Physics, Opole University of Technology, Opole, 45-370, POLAND*

[3] *Faculty of Mathematics and Natural Sciences, University of Rzeszow, Rzeszow, 35-959, POLAND*

[4] *Équipe Verres et Céramiques (V&C), ISCR CNRS UMR 6226, Université de Rennes 1, Rennes, 35042, FRANCE*

[5] *Department of sensor and semiconductor electronics, Ivan Franko National University of Lviv, 107, Tarnavskoho str., 79017 Lviv, UKRAINE*

ABSTRACT. The non-isothermal crystallization kinetics of novel $Bi_xGa_5Ge_{20}Sb_{10-x}Se_{45}Te_{20}$ (x=1,3,5,10) glasses are studied with differential scanning calorimetry method, and analysed using Frazer-Suzuki fitting function. The applicability of Johnson-Mehl-Avrami (JMA) model to describe the crystallization kinetics in these materials is verified, and JMA exponent is determined for the relevant crystallization processes. It is found, that substitution of Sb with Bi in glass composition leads to a decrease in optical gap and thermal stability of the glass, and increase in the density and crystallization activation energy for glass-ceramics formation.

Keywords: Chalcogenide glass; Crystallization; Kinetics; DSC; Optical properties

---

* Corresponding author: Faculty of Mathematics and Natural Sciences, University of Rzeszow, Rzeszow, 35-959, POLAND

E-mail address: yashpotyuk@gmail.com (Ya. Shpotyuk). Tel.: +48 17 851-8760

1. Introduction

In a past decade, the compounds of chemical elements with large spin-orbit electron coupling attracted a substantial attention because of the possibility of quantum Hall effect [1-3]. In the latter case, the spin-orbit coupling plays the same role as the external magnetic field: instead of being driven by a magnetic field, the electrons can form a quantum Hall state as a result of spin-dependent force when moving through the crystal lattice even in non-magnetic substances [2-5]. Materials which possess this effect have been named topological insulators, because they are typically insulators in the 'bulk' but have exotic metallic states present at their surfaces due to the topological order (these surface states are one of the most important properties of the topological insulators) [1-3]. For a topological insulator to form, the spin-orbit coupling must be strong enough to significantly modify the electronic structure – it should in fact be comparable to the bandgap of the material [1-3]. Historically, one of the first discovered materials with topological insulating properties was the Bi_xSb_{1-x} compound [6]. Recently, some chalcogenide stoichiometric crystals, such as Bi_2Te_3, Bi_2Se_3, Sb_2Te_3 and Sb_2Se_3, as well as mixed/doped derived compounds have been proposed as perspective three-dimensional topological insulators [7-12]. Some of them are characterized by extremely simple topological surface states described by a single gapless Dirac cone at the $k = 0$ Γ point in the surface Brillouin zone [7,8,12]. It is obvious, that Bi and Sb atoms play a key role in the formation of topological insulating properties.

Besides the prospect of forming topological insulators, incorporation of Bi or Sb into the structure of chalcogenides has a profound impact on their electrical properties [13,14]. These dopants are able to unpin the Fermi level and change the conduction from p to n type in chalcogenide glasses (which are known to be highly insensitive to metal doping [13,14]), and even cause a strong thermoelectric power effect [15,16]. The combination of these properties with high

optical transparency (extending up to ~18 μm) and non-linearity [17,18], makes Bi/Sb-containing chalcogenide alloys a very appealing multifunctional medium for numerous applications in (nano)optics and (nano)electronics [19-22]. Thus, it was discovered recently that small variation in Bi content allows fabrication of ~mm thick fully transparent or fully opaque in ~3-16 μm wavelengths range semiconducting optical media [23], which can be used for a variety of applications in IR optics and sensors. The possibility to form Bi_2Te_3, Bi_2Se_3, Sb_2Te_3 and Sb_2Se_3 (nano)crystals in amorphous matrix by a controlled crystallization (heating the glass above its glass transition temperature) or laser exposure (inducing induced fluidity or local melting of the material), opens a whole range of new metamaterials with unique physical properties [4,5,21,22].

In this paper, we introduce new glassy materials within Bi-Sb-Ga-Ge-Se-Te family with varying Bi and Sb content, which can be used as universal host matrix having potential to combine superior optical properties (like IR transparency), thermo-electric effect, different types of conductivity and topological insulating behaviour in one medium. The optical and thermal properties for these complex metamaterials are analyzed and discussed.

2. Materials and methods

The $Bi_xGa_5Ge_{20}Sb_{10-x}Se_{45}Te_{20}$ (x=1,3,5,10) glasses were prepared by conventional melt-quenching technique using high-purity elemental precursors (5N or more). Appropriate amounts of Ga, Bi, Sb, Ge, Se and Te (around 20 g in total) were vacuum-sealed in silica tube of 10 mm diameter. Then, the ampoules were heated up to 900 °C with 2 °C/min rate in a rocking furnace, homogenized for ~10-12 hours, quenched into room-temperature water from 700 °C and swiftly

moved to the preheated furnace for annealing at ~30 °C below the glass transition temperature for 3 h. For optical measurements samples were cut into discs and polished to thickness of ~1.8 mm.

The overall glassy state of the obtained materials was confirmed by the absence of crystalline reflexes in their X-ray diffraction (XRD) patterns (Fig. 1a). Nevertheless, some minor reflexes have been noticed in the XRD pattern of $Bi_{10}Ga_5Ge_{20}Se_{45}Te_{20}$ sample (Fig. 1a), which could be attributed to the formation of small-size nucleation sites right after the quench. The homogeneity and actual compositions of the prepared materials $Ga_5Ge_{20}Sb_{10}Se_{45}Te_{20}$ (Bi0), $Bi_1Ga_5Ge_{20}Sb_9Se_{45}Te_{20}$ (Bi1), $Bi_3Ga_5Ge_{20}Sb_7Se_{45}Te_{20}$ (Bi3), $Bi_5Ga_5Ge_{20}Sb_5Se_{45}Te_{20}$ (Bi5) and $Bi_{10}Ga_5Ge_{20}Se_{45}Te_{20}$ (Bi10) were verified by scanning electron microscopy (SEM) with energy-dispersive X-ray analysis (EDX), and X-ray photoelectron spectroscopy. No significant impurities or deviations (more than ±1 at.%) from nominal compositions have been found, as well as no significant inhomogeneities have been detected through SEM (Fig. 1b).

The high-energy XRD experiment was performed at the beamline 11-ID-B, Advanced Photon Source, Argonne National Laboratory, using X-rays with wavelength 0.2127 Å and position sensitive Perkin Elmer amorphous silicon image plate detector [24]. These measurements were carried out at room temperature using coarse powdered (with mortar and pestle) samples sealed in Polyimide capillaries.

Differential scanning calorimetry (DSC) measurements were performed using Mettler Toledo DSC1 instrument calibrated with Hg, In, Sn and Zn as standard elements. Bulk ~20 mg chunks of each glass were heated in 40 μl aluminum crucibles under nitrogen atmosphere at 2, 5, 10, 15, and 20 K/min constant heating rates. To assure the repeatability of the results, the DSC measurements were repeated minimum 3 times for each heating rate and for each composition (each time using a fresh sample). The DSC scan included 2 runs at the same heating rate: the first

run revealed the glass-to-supercooled liquid transition and crystallization peaks; the second run of fully crystallized glass-ceramic sample provided us with a confident baseline, which was then subtracted from the first-run curve. The crystallization peaks in the repeatable DSC data sets were fitted with Fraser-Suzuki distributions [25] in Origin. Each of these fitted curves was then integrated and normalized using Origin's intrinsic functions to obtain a fraction of crystallized volume (α).

Optical transmission spectra in the IR region were obtained with Bruker Vertex 70V spectrometer, while for the measurements in UV/VIS/NIR region the PerkinElmer LAMBDA 950 spectrophotometer was used. The VIS/NIR spectra and PARAV software [26] were used to estimate optical gaps of the glasses.

3. Results and discussion

Optical transmission spectra (Fig. 2a) and absorption coefficient, calculated in the fundamental optical absorption edge region (Fig. 2b), are typical for Se/Te-based glasses [20,27]. The samples with low Bi content are characterized by a relatively wide transmitance window (~2-16 μm), which allows a variety of IR applications. Complete substitution of Sb with Bi in glass composition leads to a full opacity of Sb-free Bi10 sample in a wide VIS-IR spectral range (transmission less than 1% for ~2 mm thick sample, not shown in Fig. 2a). This opacity is not caused by scattering, though, since no crystallites of appreciable size or other inclusions have been found in this Bi10 sample neither with XRD nor with SEM. The mechanism is, the most probably, associated with giant attenuation coefficient as suggested for similar glasses earlier [23]. The

optical gap estimated from Tauc plots using PARAV software [26] decreases with Bi content from the value of ~1 eV for Bi0 glass to ~0.7 eV for Bi5 sample (Table 1).

The DSC thermograms of the investigated glasses recorded at different heating rates $q = 2$, 5, 10, 20, 30 K/min show glass transition (Fig. 3) and crystallization (Fig. 4) features in all cases. The onset temperature of the glass transition T_g^{on} and the peak temperature of the first crystallization process T_c (both values determined for 10 K/min DSC runs) were used to calculate Dietzel criterion of glass stability $\Delta T = T_c - T_g^{on}$ [28] shown in Table 1. It is found that T_g value as determined from DSC heating curves does not change significantly with Bi addition ($T_g = 230\pm2$ °C for 10 K/min runs), except a noticable decrease for Bi10 sample ($T_g \sim 220$ °C). The activation energy of viscous flow, E_{Tg}, detemined by Ozawa method [29,30] from the data in Fig. 3 for the thermally annealed (structurally relaxed) glasses, demonstrates a maximum in compositional dependence at ~1-2 at.% of Bi (Table 1). Simultaneousely, the density of glass measured by Archimedes' method increases (Table 1) and the glass becomes less stable (smaller ΔT values) when Sb is substituted with Bi, the most unstable being the Bi10 composition with 10 at.% of Bi content (its still a glass, though, according to XRD data). Nevertheless, the T_g of all investigated samples (including Bi10) is higher than 200 °C, which makes these glasses attractive for applications in many IR instruments.

For the samples with low Bi content (x < 5 at.%) one family of crystallization peaks is observed, while for Bi5 and Bi10 samples the low-temperature crystallization emerges (Fig. 4). Fraser-Suzuki fits of DSC heating curves (Fig. 5) suggests the crystallization of at least 2 phases for the Bi-free sample (Bi0 composition), 3 phases for intermediate Bi concentrations (Bi1, Bi3 and Bi5 compositions); and as many as 5 phases for Bi10 sample. It should be noted however, that shape of real crystallization peaks can be more complicated than Fraser-Suzuki form and usually

depends on the crystallizing phase [25]. So, the proposed fits should be considered as idealized models with precautions, especially if there are weak shoulders which can be obscured by assymmetric form of Frazer-Suzuki function. They are, however, our best estimates (due to the overlapped crystallization processes of unknown nature) to determine the crystallization temperatures and activation energies of crystallization processes.

Johnson-Mehl-Avrami (JMA) nucleation-growth model is usually used to study the non-isothermal crystallization kinetics with DSC [31,32]. The fraction of crystallized volume α during non-isothermal crystal growth from preexisting nuclei can be determined from [31,32]:

$$\frac{d\alpha}{dt} = Af(\alpha)e^{\left(-\frac{E_a}{RT}\right)}$$

(1)

$$\alpha = \frac{1}{\Delta H_c}\int_0^T \phi dT \qquad .$$

(2)

Here ϕ is the specific heat flow measured with DSC (W/g) and ΔH_c is the total enthalpy change associated with the crystallization process; the pre-exponential factor A and activation energy E_a are kinetic parameters that should not depend on the temperature T and α; and

$$f(\alpha) = m(1-\alpha)[-\ln(1-\alpha)]^{1-1/m}$$

(3)

is an algebraic expression of the JMA model [31,32].

The JMA exponent m is a characteristic parameter related to a crystal forming morphology: $m \sim 1$ means predominant surface crystallization, $m \sim 3$ corresponds to three-dimensional bulk crystallization, and $m \geq 4$ usually describes the crystallization processes occurring with increasing nucleation rate [33].

A simple test for the applicability of JMA model is based on the analysis of probe functions [31]:

$$y(\alpha) = \phi e^{\left(-\frac{E_a}{RT}\right)} \tag{4}$$

$$z(\alpha) = \phi T^2 \tag{5}$$

For JMA model to be valid, the maximum of $z(\alpha)$ function should occur around $\alpha = 0.63 \pm 0.02$ value in the non-isothermal crystallization conditions [31].

The fits with Fraser-Suzuki distribution function were used to build $z(\alpha)$ plots for the resolved crystallization processes. As could be seen from Fig. 6, only peaks III of Bi1 and Bi3 samples, as well as peak II of Bi5 sample have their $z(\alpha)$ maxima at roughly $\alpha \sim 0.63$ value (taking into account a reasonable accuracy achievable with DSC instrument for rapidely crystallizing phases). So, only these crystallization processes can be potentially described with JMA model of crystallization. The JMA exponent m estimated from the double-logarithm plots (Fig. 7) is found to be close to 3 for the peaks III of Bi1 and Bi3 samples, and approximately 7 for the peak II of Bi5 sample. The latter means crystallization processes with increasing nucleation rate [33].

The activation energies of crystallization (E_a) calculated using Ozawa's plots (ln q vs 1000/T) [29,30] show overall increase with Bi content (Table 2). This can be explained by the fact that onset of crystallization shifts to lower temperatures in Bi-contaning glasses, where higher viscosity of supercooled liquid imposes more constraints on structural rearrangements needed for crystallization to occur. Simultaneously, crystallization peaks become sharper (Fig. 4), which means more rapid crystallization of the phases in glasses with greater Bi content. This result is of significant importance for the application of these materials in phase-change memory devices.

The nature of the crystallizing phases in each case requires further thorough investigations using combination of Raman/IR spectrocopy, electron microscopy, XRD analysis, and such complementary structural probes as X-ray photoelectron spectroscopy and extended X-ray absorption fine structure spectroscopy. Nevertheless, on the basis of previous studies [34], we expect that in the low temperature region the predominant crystallization of Bi-based compounds (like Bi_2Te_3, Bi_2Se_3 or Bi_2SeTe_2) should occur. In the high-temperature range beyond ~320 ℃, the crystallization processes should rely mostly on the crystallization of stable Ge- and Sb-based chalcogenide phases [34].

4. Conclusions

The Ga-Ge-Se-Te matrix is found to be quite suitable for the incorporation of high concentration of Sb and Bi (up to 10 at.%), while preserving the overall glassy state. Substitution of Sb with Bi leads to an increase in density of the glass, a decrease in the optical gap of these materials and, finally, to the complete opacity of ~2 mm thick sample with 10 at.% of Bi in a wide visible and infrared range of spectrum. Analysis of the crystallization kinetics reveals that only few crystallization processes can be described with Johnson-Mehl-Avrami crystallization model, while majority of them do not pass JMA applicability test (at least per Frazer-Suzuki fits). The activation energies of crystallization show a tendency to increase with Bi content, which is associated with an overall shift of the crystallization processes to lower temperatures. Glass-ceramics formation by crystallization becomes more rapid in Bi-rich glasses, but simultaneously their Dietzel criterion of glass stability decreases. Owing to the obtained results, the developed glass matrix can be considered for multifunctional applications in IR optics, photonics, phase-change memory devices, and sensors.

Acknowledgements

References

[1]   J.E. Moore, The birth of topological insulators, Nature 464 (2010) 194-198.

[2]   Y. Ando, Topological insulator materials, J. Phys. Soc. Jpn. 82 (2013) 102001.

[3]   T.O. Wehling, A.M. Black-Schaffer, A.V. Balatsky, Dirac materials, Adv. Phys. 63 (2014) 1–76.

[4]   A. Agarwala, V.B. Shenoy, Topological Insulators in Amorphous Systems, Phys. Rev. Lett. 118 (2018) 236402.

[5]   N.P. Mitchell, L.M. Nash, D. Hexner, A.M. Turner, W.T. M. Irvine, Amorphous topological insulators constructed from random point sets, Nature Physics (2018). doi:10.1038/s41567-017-0024-5.

[6]   D. Hsieh, Y. Xia, L. Wray, D. Qian, A. Pal, J. H. Dil, J. Osterwalder, F. Meier, G. Bihlmayer, C. L. Kane, Y. S. Hor, R. J. Cava, M. Z. Hasan, Observation of Unconventional Quantum Spin Textures in Topological Insulators, Science 323 (2009) 919-922.

[7] H. Zhang, C.-X. Liu, X.-L. Qi, X. Dai, Zh. Fang, Sh.-Ch. Zhang, Topological insulators in Bi$_2$Se$_3$, Bi$_2$Te$_3$ and Sb$_2$Te$_3$ with a single Dirac cone on the surface, Nature Physics 5 (2009) 438-442.

[8] Y.L. Chen, J. G. Analytis, J.-H. Chu, Z. K. Liu, S.-K. Mo, X. L. Qi, H. J. Zhang, D. H. Lu, X. Dai, Z. Fang, S. C. Zhang, I. R. Fisher, Z. Hussain, Z.-X. Shen, Experimental realization of a three-dimensional topological insulator, Bi$_2$Te$_3$, Science 325 (2009) 178–181.

[9] P. Seifert, K. Vaklinova, S. Ganichev, K. Kern, M. Burghard, A.W. Holleitner, Spin Hall photoconductance in a three-dimensional topological insulator at room temperature, Nature Commun. 9 (2018) 331.

[10] L.-X. Qin, X.-C. Pan, F.-Q. Song, L. Zhang, Zh.-H. Sun, M.-Q. Li, P. Gao, B.-C. Lin, S.-M. Huang, R. Zhu, J. Xu, F. Lin, H.-Z. Lu, D. Yu, Zh.-M. Liao, Confined-path interference suppressed quantum correction on weak antilocalization effect in a BiSbTeSe$_2$ topological insulator, Appl. Phys. Lett. 112 (2018) 032102.

[11] S.W. Cho, K.-Ch. Kim, S.K. Kim, B. Cheong, J.-S. Kim, S. Lee, Suppression of bulk conductivity and large phase relaxation length in topological insulator Bi$_{2-d}$Sn$_d$Te$_3$ epitaxial thin films grown by Metal-Organic Chemical Vapor Deposition (MOCVD), J. Alloys and Compounds 723 (2017) 942-947.

[12] D. Usanmaz, P. Nath, C. Toher, J.J. Plata, R. Friedrich, M. Fornari, M. B. Nardelli, S. Curtarolo. Spinodal Superlattices of Topological Insulators. Chem. Mater. 2018 (in press).

[13] C. Vautier, Role of metal impurity "Bi" in amorphous chalcogenide semiconductors, Solid State Phenom. 71 (2000) 249-270.

[14] A. Feltz, Amorphous inorganic materials and glasses, VCH Publishers, New York, 1993.

[15] G. Singh, J. Sharma, A. Thakur, N. Goyal, G. S. S. Saini, S. K. Tripathi, Effect of bismuth on the electrical properties of a-$Ge_{20}Se_{80}$ glasses, J. Optoelectron. Adv. Mater. 7 (2005) 2069-2076.

[16] Y. Liu, Sh. Yuan, J. Xie, F. Shangguan, J. Ren, G. Chen, A Study on Crystallization Kinetics of Thermoelectric Bi_2Se_3 Crystals in Ge–Se–Bi Chalcogenide Glasses by Differential Scanning Calorimeter, J. Am. Ceram. Soc. 96, *7* (2013) 2141–2146.

[17] A. Zakery, and S.R. Elliott, Optical nonlinearities in chalcogenide glasses and their applications, Springer-Verlag, Berlin, Heidelberg, 2007.

[18] J.S. Sanghera, I.D. Aggarwal, Active and passive chalcogenide glass optical fibers for IR applications: a review, J. Non-Cryst. Solids 256&257 (1999) 6-16.

[19] B. J. Eggleton, B. Luther-Davies, K. Richardson, Chalcogenide photonics, Nature Photonics 5 (2011) 141–148.

[20] J-L. Adam and X. Zhang (Eds), Chalcogenide Glasses: Preparation, properties and application, Woodhead Publishing series in Electronic and Optical Materials No.44, 2014.

[21] M.-S. Lim, S.-H. Jhi, Thermoelectric properties of thin film topological insulators: A first-principles study, Solid State Communications 270 (2018) 22-25.

[22] Y. Liu, Y. Zhang, S. Ortega, M. Ibáñez, K.H. Lim, A. Grau-Carbonell, S. Martí-Sánchez, K.M. Ng, J. Arbiol, M.V. Kovalenko, D. Cadavid, A. Cabot, Crystallographically Textured Nanomaterials Produced from the Liquid Phase Sintering of $Bi_xSb_2–xTe_3$ Nanocrystal Building Blocks, Nanoletters (2018). doi**:** 10.1021/acs.nanolett.8b00263.

[23] R. Golovchak, Ya. Shpotyuk, J. Szlęzak, A. Dziedzic, A. Ingram, J. Cebulski, Giant VIS-IR light attenuation effect in nanostructured narrow-bandgap glasses, Opt. Lett. 43 (2018) 387-390.

[24] P. J. Chupas, X. Y. Qui, J. C. Hanson, P. L. Lee, C. P. Grey, and S. J. L. Billinge, Rapid-acquisition pair distribution function (RA-PDF) analysis, J. Appl. Cryst. 36 (2003) 1342-1347.

[25] A. Perejon, P.E. Sanchez-Jimenez, J.M. Criado, L.A. Perez-Maqueda, Kinetic Analysis of Complex Solid-State Reactions. A New Deconvolution Procedure, J. Phys. Chem. B 115 (2011) 1780–1791.

[26] A. Ganjoo, R. Golovchak, Computer program PARAV for calculating optical constants of thin films and bulk materials: Case study of amorphous semiconductors, J. Optoelectron. Adv. Mater. 10, 6 (2008) 1328-1332.

[27] S. Cui, R. Chahal, Ya. Shpotyuk, C. Boussard, J. Lucas, F. Charpentier, H. Tariel, O. Loreal, V. Nazabal, O. Sire, V. Monbet, Z. Yang, P. Lucas, B. Bureau, Selenide and telluride glasses for mid-infrared bio-sensing, Proc. SPIE, 8938 (2014) 893805-1-9.

[28] A. Dietzel, Glass Structure and Glass Properties, Glasstech. Ber. 22 (1968) 41-50.

[29] T. Ozawa, Nonisothermal kinetics of crystal growth from pre-existing nuclei, Bull. Chem. Soc. Jpn. 57 (1984) 639-643.

[30] T. Ozawa, A new method of analyzing thermogravinetric data, Bull. Chem. Soc. Japan 38 (1965) 1881-1886.

[31] J. Malek, Kinetic analysis of crystallization processes in amorphous materials, Thermochim. Acta 355 (2000) 239-253.

[32] J. Sestak, Thermophysical Properties of Solids. Their Measurements and Theoretical Analysis, Elsevier, Amsterdam, 1984.

[33] K. Matusita, T. Komatsu, R. Yokota, Kinetics of non-isothermal crystallization process and activation energy for crystal growth in amorphous materials, J. Mater. Sci. 19 (1984) 291-294.

[34] L. Saturday, C. Johnson, A. Thai, J. Szlęzak, Ya. Shpotyuk, R. Golovchak, Devitrification of Bi- and Ga-containing germanium-based chalcogenide glasses, J. Alloys Compd. 674 (2016) 207-217.

Table 1. Dietzel criterion of glass stability $\Delta T = T_c - T_g{}^{on}$ [28], calculated for the investigated $Bi_xGa_5Ge_{20}Sb_{10-x}Se_{45}Te_{20}$ glasses using DSC curves recorded at 10 K/min heating rate (T_c is the peak value of the earliest crystallization peak, $T_g{}^{on}$ is the onset value of glass transition); density ρ; estimated optical gap E_g; and activation energies of viscous flow E_{Tg}, averaged for Ozawa's plots of onset and midpoint T_g values.

Parameter Sample	$T_g{}^{on}$, °C (±1)	T_c, °C (±1)	ΔT, °C (±1)	E_{Tg}, kJ/mol (±50)	E_g, eV (±0.05)	ρ, g/cm^3 (±0.005)
$Ga_5Ge_{20}Sb_{10}Se_{45}Te_{20}$	231	381	150	310	1.00	4.983
$Bi_1Ga_5Ge_{20}Sb_9Se_{45}Te_{20}$	230	373	143	630	0.85	5.043
$Bi_3Ga_5Ge_{20}Sb_7Se_{45}Te_{20}$	228	346	118	510	0.80	5.100
$Bi_5Ga_5Ge_{20}Sb_5Se_{45}Te_{20}$	229	303	74	360	0.71	5.226
$Bi_{10}Ga_5Ge_{20}Se_{45}Te_{20}$	218	261	43	282	n/a	5.441

Table 2. Average activation energy of crystallization E_a calculated for the investigated materials using Ozawa's plots [29,30].

	E_a	Peak I kJ/mole (± 5)	Peak II kJ/mole (± 5)	Peak III kJ/mole (± 5)	Peak IV kJ/mole (± 5)	Peak V kJ/mole (± 5)
Sample						
$Ga_5Ge_{20}Sb_{10}Se_{45}Te_{20}$		134	144			
$Bi_1Ga_5Ge_{20}Sb_9Se_{45}Te_{20}$		137	138	163		
$Bi_3Ga_5Ge_{20}Sb_7Se_{45}Te_{20}$		167	195	206		
$Bi_5Ga_5Ge_{20}Sb_5Se_{45}Te_{20}$		241	254	257		
$Bi_{10}Ga_5Ge_{20}Se_{45}Te_{20}$		271	283	300	228	242
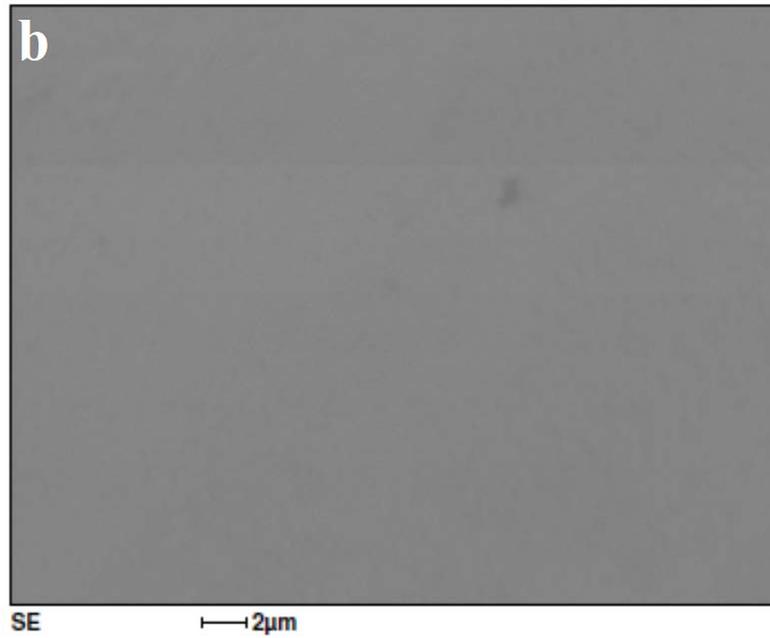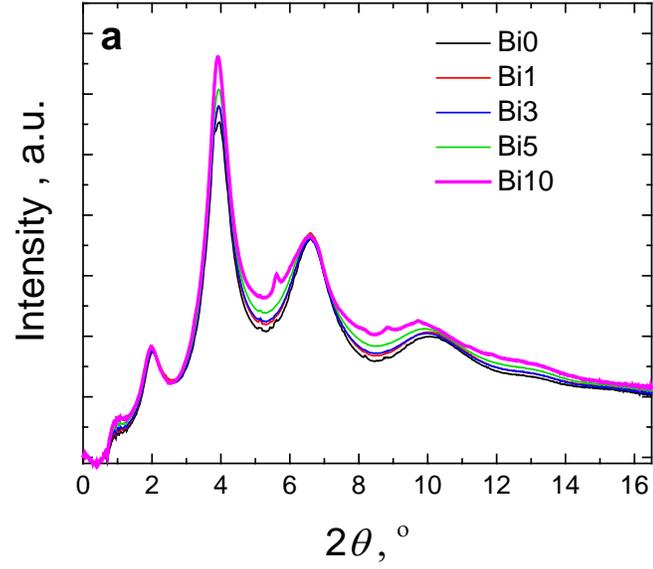
Fig. 1. (a) High-energy XRD patterns of the investigated $Bi_xGa_5Ge_{20}Sb_{10-x}Se_{45}Te_{20}$ glasses; (b) SEM picture of a fresh fracture of as-prepared Bi10 sample.
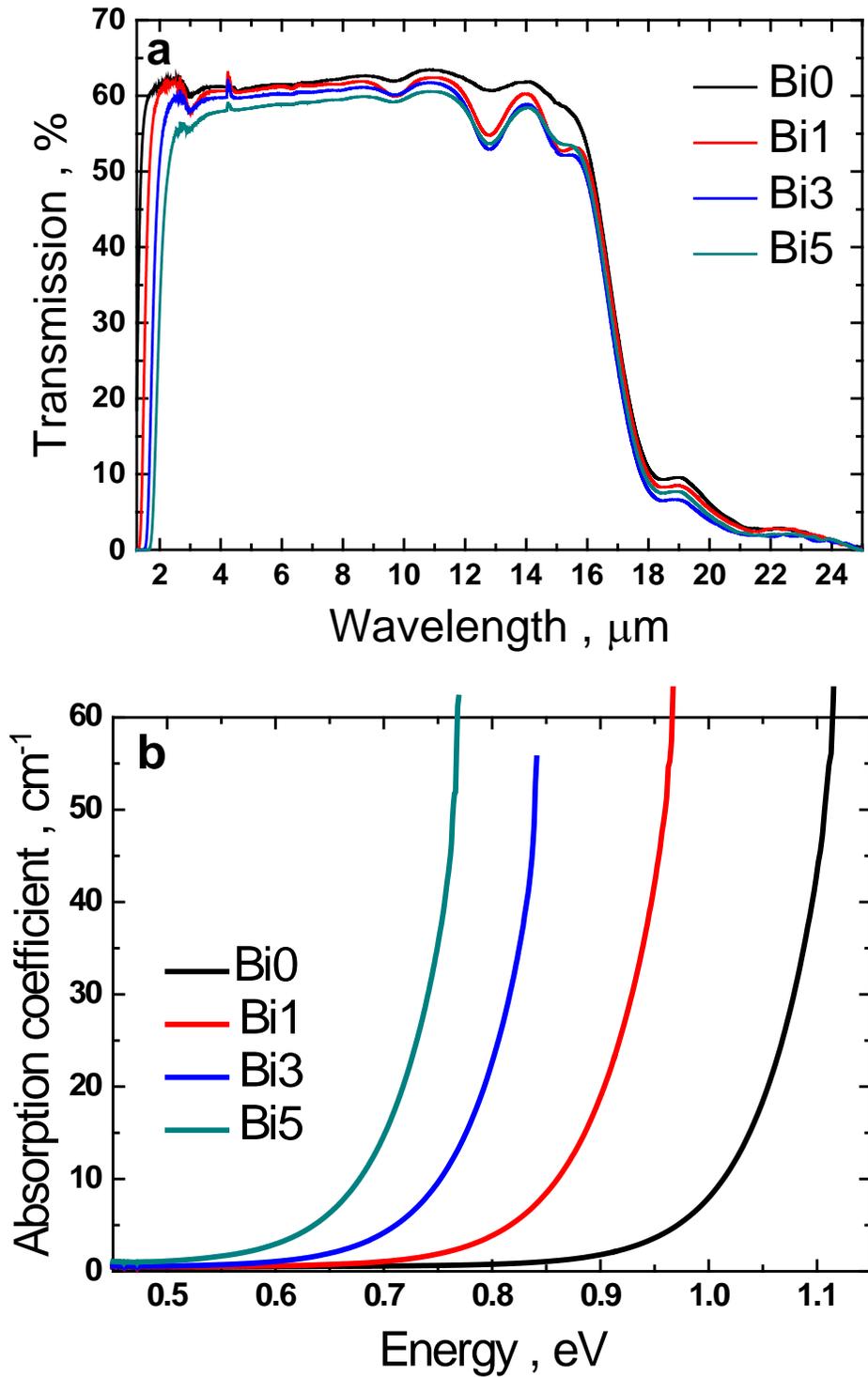
Fig. 2. Transmission (a) and fundamental optical absorption (b) spectra of $Bi_xGa_5Ge_{20}Sb_{10-x}Se_{45}Te_{20}$ glasses (Bi10 sample is not shown due to its complete opacity in this optical region).
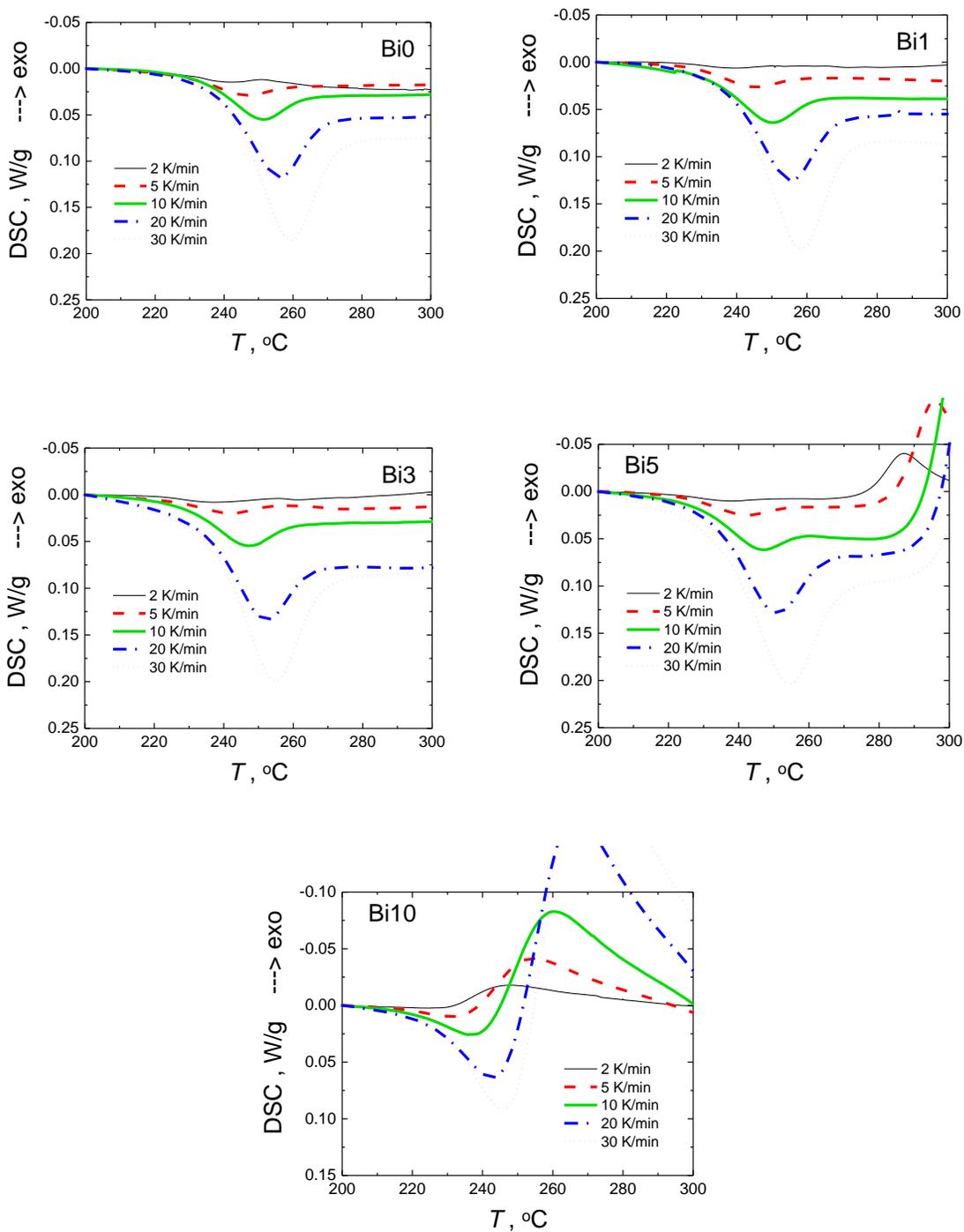
Fig. 3

Fig. 3. DSC scans at different heating rates for $Bi_xGa_5Ge_{20}Sb_{10-x}Se_{45}Te_{20}$ glasses, showing glass transition region.
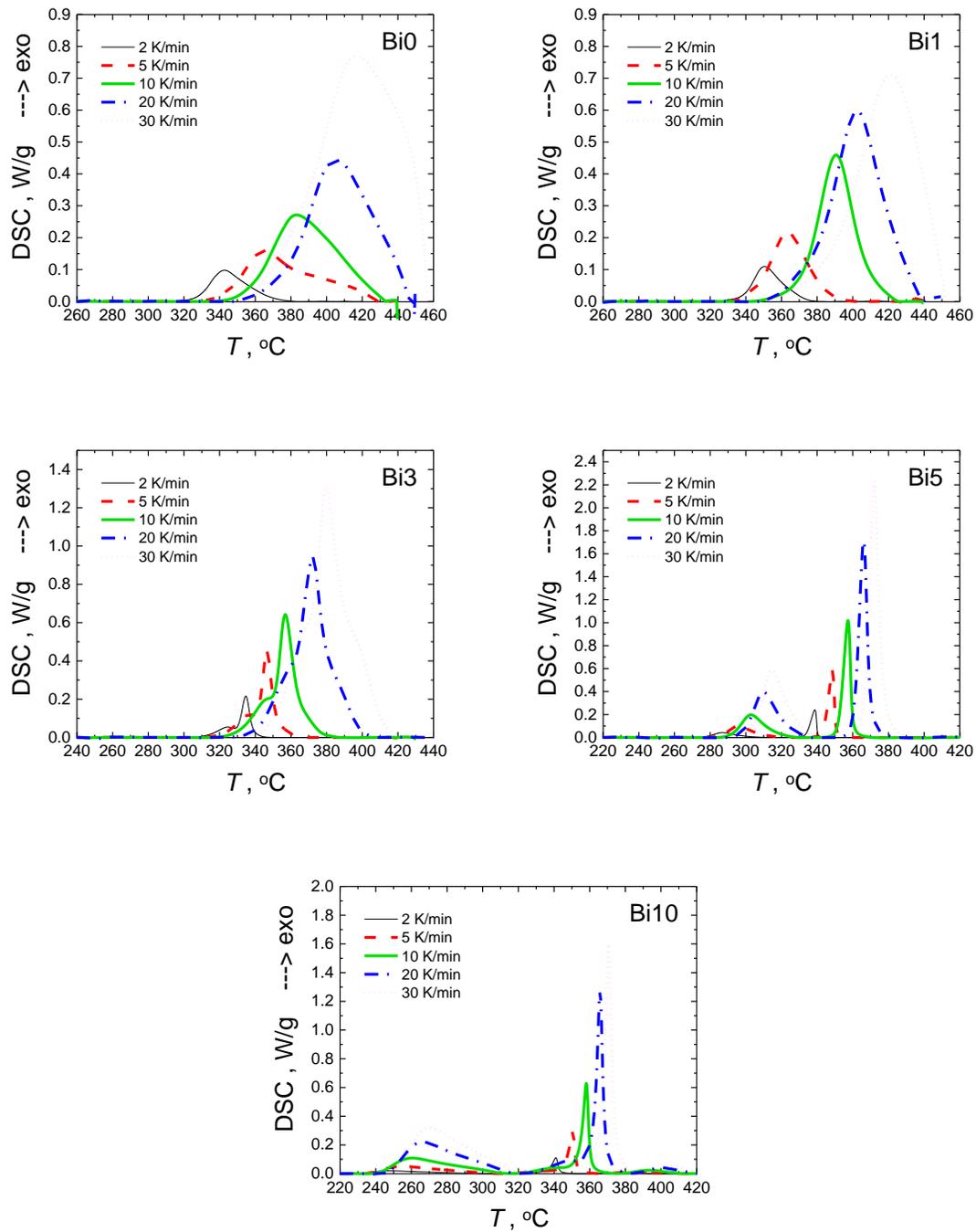
Fig. 4. DSC scans at different heating rates for $Bi_xGa_5Ge_{20}Sb_{10-x}Se_{45}Te_{20}$ glasses, showing crystallization region.
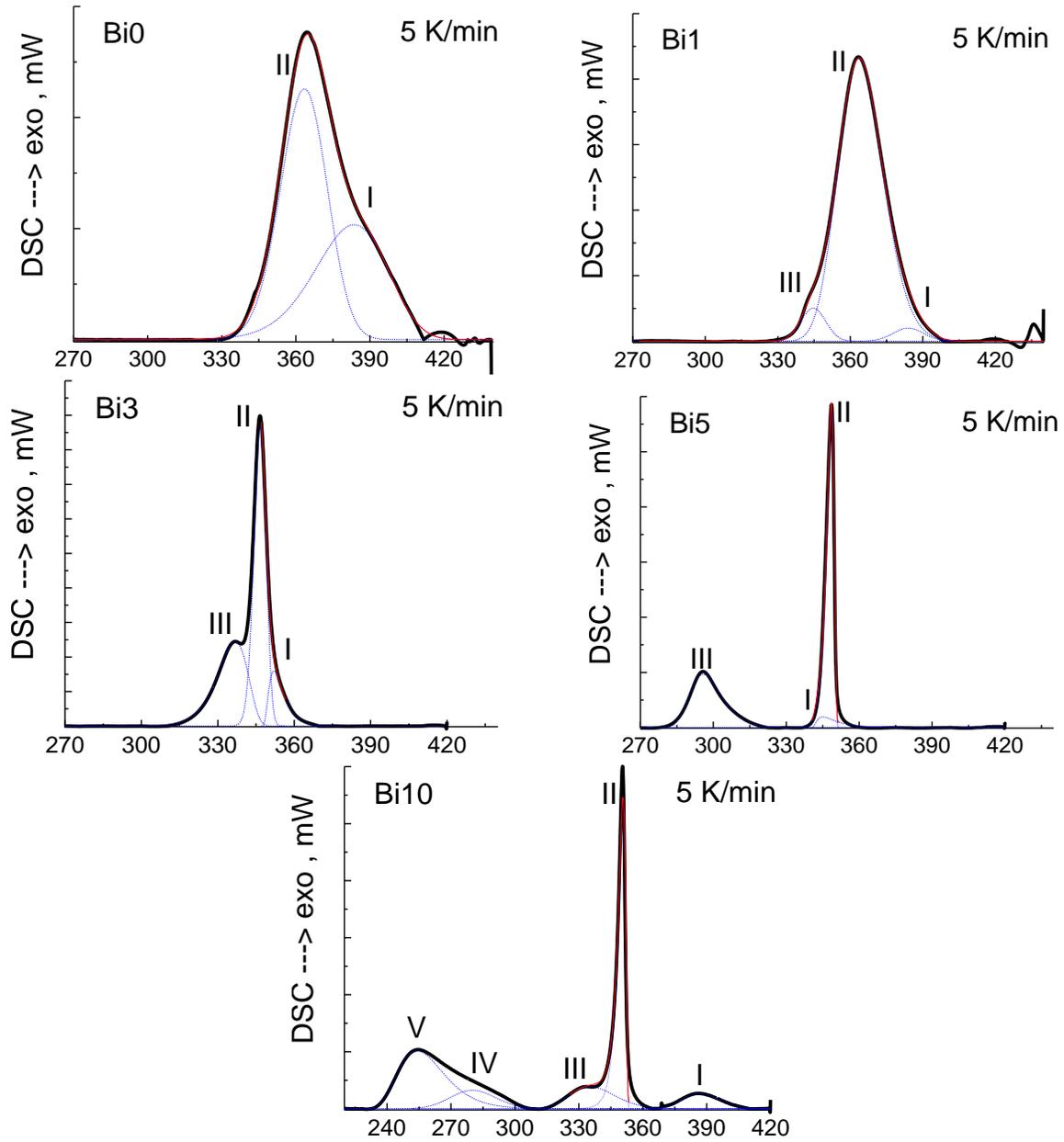
Fig. 5. Example of Fraser-Suzuki fittings for DSC curves of $Bi_xGa_5Ge_{20}Sb_{10-x}Se_{45}Te_{20}$ glasses recorded at 5 K/min heating rate in the crystallization region.
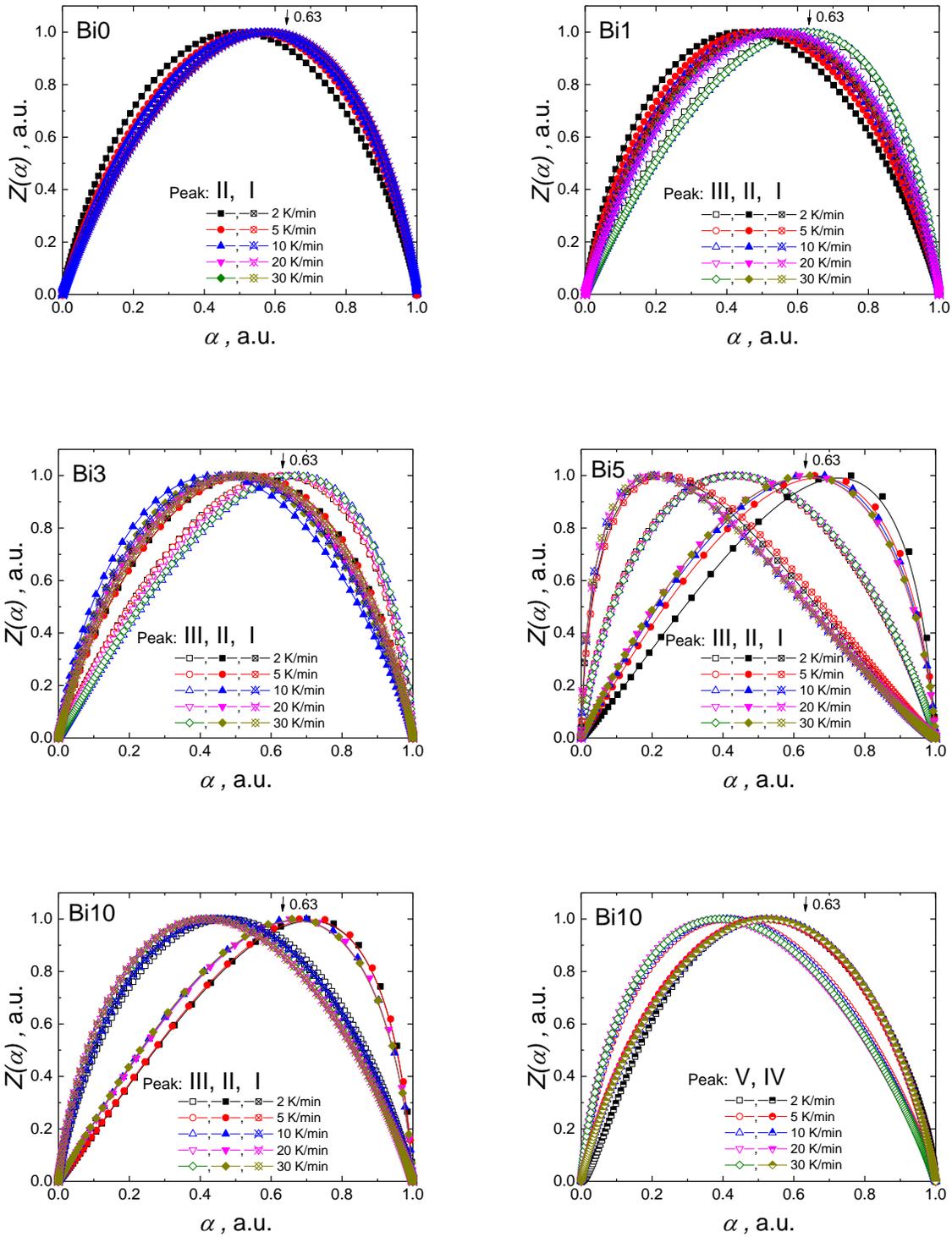
Fig. 6. The $z(\alpha)$ functions built of Frazer-Suzuki fits for crystallization regions of $Bi_xGa_5Ge_{20}Sb_{10-x}Se_{45}Te_{20}$ samples to check the applicability of JMA equation.
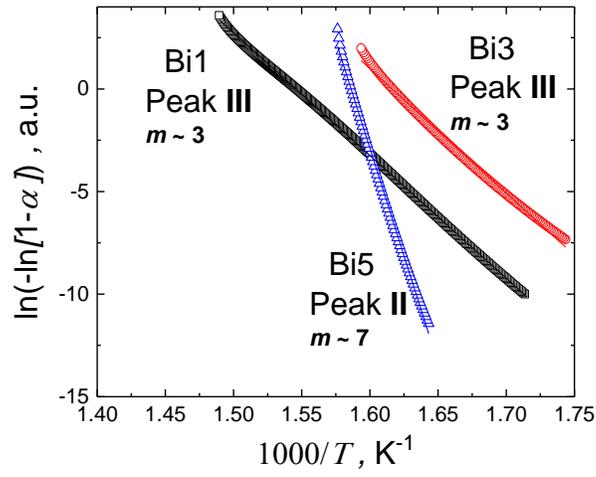
Fig. 7. Plots for JMA exponent determination for selected crystallization processes deemed to be described by JMA model.